

**University of Nebraska - Lincoln**  
**DigitalCommons@University of Nebraska - Lincoln**

---

Computer Science and Engineering: Theses,  
Dissertations, and Student Research

Computer Science and Engineering, Department of

Winter 5-2019

# Image Processing Algorithms for Elastin Lamellae Inside Cardiovascular Arteries

Mahmoud Habibnezhad

*University of Nebraska-Lincoln*, mahmoud@huskers.unl.edu

Follow this and additional works at: <https://digitalcommons.unl.edu/computerscidiss>

Part of the [Computer Engineering Commons](#), and the [Computer Sciences Commons](#)

---

Habibnezhad, Mahmoud, "Image Processing Algorithms for Elastin Lamellae Inside Cardiovascular Arteries" (2019). *Computer Science and Engineering: Theses, Dissertations, and Student Research*. 168.  
<https://digitalcommons.unl.edu/computerscidiss/168>

This Article is brought to you for free and open access by the Computer Science and Engineering, Department of at DigitalCommons@University of Nebraska - Lincoln. It has been accepted for inclusion in Computer Science and Engineering: Theses, Dissertations, and Student Research by an authorized administrator of DigitalCommons@University of Nebraska - Lincoln.

IMAGE PROCESSING ALGORITHMS FOR ELASTIN LAMELLAE INSIDE  
CARDIOVASCULAR ARTERIES

by

Mahmoud Habibnezhad

A THESIS

Presented to the Faculty of  
The Graduate College at the University of Nebraska  
In Partial Fulfilment of Requirements  
For the Degree of Master of Science

Major: Computer Science

Under the Supervision of Professor Peter Z. Revesz

Lincoln, Nebraska

May, 2019

IMAGE PROCESSING ALGORITHMS FOR ELASTIN LAMELLAE INSIDE  
CARDIOVASCULAR ARTERIES

Mahmoud Habibnezhad, M.S.

University of Nebraska, 2019

Adviser: Peter Z. Revesz

Automated image processing methods are greatly needed to replace the tedious, manual histology analysis still performed by many physicians. This thesis focuses on pathological studies that express the essential role of elastin lamella in the resilience and elastic properties of the arterial blood vessels. Due to the stochastic nature of the shape and distribution of the elastin layers, their morphological features appear as the best candidates to develop a mathematical formulation for the resistance behavior of elastic tissues. However, even for trained physicians and their assistants, the current measurement procedures are highly error-prone and prolonged. This thesis successfully integrates such techniques in an image processing application that results in increased speed and accuracy. In particular, the image processing algorithms can identify and count the elastin lamella within a 10% error on average. Modifications of the elastin-lamella counting algorithm can also recognize artery boundaries and calculate the continuity index and the distribution of elastin layers.

## DEDICATION

*To my lovely wife, Sara.*

## ACKNOWLEDGMENTS

I would like to express my gratitude and appreciation to my thesis advisor Prof. Peter Revesz of the department of computer science at the University of Nebraska-Lincoln. Prof. Revesz was always ready for my questions about my research or writing. Not only his great ideas steered me in the right direction, but without his support, the completion of this work was not possible.

I would also like to thank the experts who provided me with access to the thirty-one histology images and were involved in the Gold Standard (GS) acquisition process for this research project: Dr. Alexey Kamenskiy, Associate Professor of Department of Surgery at Nebraska Medical Center and Majid Jadidi, Ph.D. Student of the Department of Mechanical Engineering at University of Nebraska-Lincoln. Without their passionate participation and help, the validation of my image processing application could not have been successfully conducted.

I would also like to acknowledge Prof. Ashok Samal and Dr. Chris Bourke from the Computer science department at the University of Nebraska-Lincoln as the second readers of this thesis, and I am gratefully indebted to them for their precious comments on this thesis.

Finally, I must express my very profound gratitude to my wonderful wife, Sara, for providing me with unfailing support and continuous encouragement throughout my years of study and through the process of researching and writing this thesis. This accomplishment would not have been possible without you. Thank you.

Author

Mahmoud Habibnezhad

## Table of Contents

<b>List of Figures</b>	vii
<b>List of Tables</b>	ix
<b>1 INTRODUCTION</b>	1
1.1 Overview . . . . .	1
1.2 Problem statement . . . . .	2
1.3 Objective . . . . .	4
1.4 Contribution . . . . .	4
1.5 Outline of the Thesis . . . . .	4
<b>2 BACKGROUND CONCEPTS AND RELATED WORKS</b>	6
2.1 Importance of Elastin Lamella in Defining the Micromechanics of Arterial Vessels . . . . .	6
2.2 Morphological Properties of Elastin Fibers and Lamella Inside Cardiovascular Blood Vessels . . . . .	7
2.3 Automation in Pathology by Using Image Processing Techniques . .	8
<b>3 ALGORITHMS</b>	14
3.1 Algorithm for Extracting Elastin-Related Features . . . . .	14
3.2 Development Platform . . . . .	17

<b>3.3 Image Processing Techniques . . . . .</b>	<b>17</b>
<b>3.3.1 Tiff-Extracting Feature . . . . .</b>	<b>17</b>
<b>3.3.2 Thinning and Thresholding . . . . .</b>	<b>18</b>
<b>3.3.3 Contour Analysis . . . . .</b>	<b>19</b>
<b>3.3.4 Outlier Removal . . . . .</b>	<b>20</b>
<b>3.3.5 Continuity Measurement . . . . .</b>	<b>20</b>
<b>3.3.6 Best-Fit Polynomial . . . . .</b>	<b>21</b>
<b>3.3.7 Feature Extraction . . . . .</b>	<b>30</b>
<b>3.3.7.1 Layer Counting . . . . .</b>	<b>33</b>
<b>3.3.7.2 Space Measurement between Elastin Lamella . . . . .</b>	<b>35</b>
<b>4 METHODOLOGY . . . . .</b>	<b>37</b>
<b>4.1 Data Source . . . . .</b>	<b>37</b>
<b>4.1.1 Artery Samples . . . . .</b>	<b>37</b>
<b>4.2 Histology Image Analyzer Application . . . . .</b>	<b>38</b>
<b>4.3 Gold Standard (GS) . . . . .</b>	<b>38</b>
<b>5 RESULTS AND DISCUSSION . . . . .</b>	<b>40</b>
<b>6 CONCLUSIONS AND FUTURE WORK . . . . .</b>	<b>46</b>
<b>6.1 Conclusion . . . . .</b>	<b>46</b>
<b>6.2 Limitation and Future work . . . . .</b>	<b>46</b>
<b>Bibliography . . . . .</b>	<b>48</b>

## List of Figures

3.1	sample histology image of an arterial blood vessel . . . . .	19
3.2	the result of black and white thresholding on the blood vessel sample .	19
3.3	the result of black and white thresholding on the blood vessel sample .	21
3.4	A schematic picture of an arteries' walls analyzed with a perpendicular line relative to the blood vessel's direction. Here, the line probe is oriented perpendicular to the boundaries of the vessel. On the other hand, in the left picture, the line probe is not perpendicular to the boundaries, and therefore, not accurately count the number of elastin fibers. . . . .	23
3.5	A schematic picture of an arteries' walls analyzed with a diagonal line. Here, the line probe is not perpendicular to the boundaries, and therefore, not accurately count the number of elastin fibers. . . . .	24
3.6	Perpendicular line problem due to the inconsistency between the boundary points. At the top, you can see the boundary points used to draw perpendicular lines. At the bottom, the perpendicular lines have been drawn by using a least-square best-fit polynomial of degree 6 that passes through the same boundary points. The red-colored points are the mapped points on the best-fit curve. . . . .	25

3.7	The perpendicular lines to the fitted curve along with the points on the curve by which the line probes drew . . . . .	26
3.8	The curve-fitting polynomial without any scale factor implementation .	28
3.9	The curve-fitting polynomial with the scale factor implementation. Here SF is 10. . . . .	28
3.10	The curve-fitting polynomial with the scale factor implementation. Here SF is 100. . . . .	29
3.11	The binary image of the artery sample with the two boundary fitting curves . . . . .	29
3.12	The binary image of the artery sample in which the bounding box and the line probe have been illustrated . . . . .	30
3.13	A ring-shaped cross-section of an artery . . . . .	31
3.14	The image of a ring-shaped sample of an artery bounded with best-fitted curves . . . . .	32
3.15	A semi-irregular distribution of elastin lamella represented by contours	34
3.16	The result of elastin lamella detection technique on an artery histology image. In this figure, the tiny red-colored circles (dots) show the non-elastin layers, while the green-colored circles show the elastin lamella. .	35
5.1	This is an example of a bad elastin detection. The red arrows (small head) show false detection, and the orange arrows (big head) show false skips. . . . .	43
5.2	Detected contours of black pixels related to a part of a histology image demonstrated earlier on Figure 5.1 . . . . .	44

## List of Tables

4.1	Contingency table for elastin-layer detection . . . . .	38
5.1	A part of the programs results for the selected thirty-one histology images corresponding to axial-shape specimens of arteries . . . . .	41
5.2	accuracy and consistency test results for the application performance in detecting elastin lamella . . . . .	42

## Chapter 1

### INTRODUCTION

#### 1.1 Overview

Based on the World Health Organization, cardiovascular diseases account for a large portion of mortalities. One of the leading causes of cardiovascular disorders is changes in the mechanical properties of the arterial vessels. Irregular changes in the diameter of arteries, known as ascending aorta dilation, can be the start of a severe vascular disorder. Another dangerous consequence of ascending aorta dilation is the increase risk of aortic rupture. An aneurysm, the situation in which the diameter of the aorta becomes greater than twice the average diameter calculated by the age and height of the patient, demonstrates one of the extreme cases of these vascular complications [22].

Based on numerous pathological studies, elastin and collagens are the two main microstructural elements of blood vessels defining their resilience and elastic behaviors. Accordingly, Okamoto et al. showed that the elastic properties of arteries, mainly characterized by elastin layers, can be a prominent factor in constructing advanced mathematical models of blood vessels. [18]. These mathematical models can describe and predict the behavior of an artery under various loads. They are suitable for investigating any potential associations with

patients vascular health status and helpful throughout different stages of clinical treatments for vascular disorders.

Usually, due to the stochastic shape of elastin lamella, their morphological properties are the best candidates to construct mathematical models of arteries. Therefore, it is important to study elastin layers properties extensively. Since histology images are great for analysis of the microanatomy of cells and micro-scale tissues, most of the biomedical examinations of elastin lamella are performed by utilizing these high-resolution images.

## 1.2 Problem statement

The immense size and number of pixels of histology images make the manual analysis of such images time-consuming, tedious, and error-prone. Also, the preparation of these images such as reading, cropping, and storing the file can be quiet challenging. By examining the typical procedure of a specialist who counts the number of elastin layers from a histology image, the inefficiencies are apparent. Due to the optimal compression technique used in tiff files for high maintainability and quality preservability, most of the high-resolution images will be stored in this format. Usually, these files contain several directories each associated with a roster of pixels pertaining to the pictures of the tissue. Therefore, the first step towards studying the distributions and numbers of elastin lamella would be to extract the pixels from the corresponding directory. Then, rearrange the pixels into a matrix, and finally store them in a jpeg, or jpg format. Afterwards, by utilizing a powerful image viewing software, the converted image should be opened and then cropped, so that the modified image would be ready for analysis. Once the image is ready, the specialist needs to zoom into the media layer of the artery, divide the layer into

at least five sections and count the number of elastin fibers for each section. The background might make it harder for the operator to count the elastin lamellae. Furthermore, accurate measurements of the distances between the elastin lamellae cannot be performed solely based on a person's judgment. They need software with image measurement capability to obtain the distances between elastin layers, and consequently, their distributions along the thickness of the blood vessels wall. These difficulties can be magnified if the number of images increases, to the point that it would be impossible for the operator to manually or even semi-manually analyze the images.

This manual procedure was an example of a general analysis case. In other words, the number of elastin lamella inside the medial layer and their corresponding distributions are two of many other important parameters used in the morphological studies. Some of these parameters are listed below:

1. Connectivity index of elastin lamellae,
2. Density of black pixels associated with elastin layers
3. Disarray measurement of elastin fibers (mostly used for 3D orientation calculation)
4. Dispersive index.

As can be seen, the manual analysis of high-resolution images can be quite staggering, suggesting a need for an image processing application that can alleviate this prolonged process. The development of such an application can be valuable in reducing human errors and a big step towards the automation of geometric morphological analysis.

### **1.3 Objective**

By proposing a new image processing application furnished with efficient and innovative algorithms, this study aims to fully automate the feature extraction of elastin layers in arteries. Accordingly, the result of such an application will be compared with the Gold Standard (GS) acquired from the professionals judgment regarding the number of elastin lamellae inside arteries.

### **1.4 Contribution**

This thesis presents an innovative approach towards complete accessibility to the 'elastin' pixels of histology images of arteries. Accordingly, by implementing efficient image processing algorithms, our application is capable of extracting the location and intensity of the 'elastin' pixels within an arterial histology image. Based on the result of this study, our proposed image processing algorithms show adequate accuracy in calculating the morphological features of elastin lamella. Since many clinical examinations and treatments are contingent upon the elastin properties of cardiovascular blood vessels, our application can be utilized in many of these clinical trials. Also, the presented application can create a foundation upon which other related image processing techniques can be built.

### **1.5 Outline of the Thesis**

The rest of the thesis is organized as follows: Chapter 2 describes the relevant work regarding the cardiovascular health issues, the importance of blood vessels microstructural elements to define the elastic properties and resilience of the blood vessels. Finally, the similar image processing approaches towards automation

in studying and analyzing histology images has been introduced. Chapter 3 is dedicated to an in-depth explanation of the developed Histology-Image Analyzer application and all the implemented image processing techniques. Following the explanation of the application in Chapter 4, a brief description of the database containing all the processed histology images is presented. Also, all the procedures carried out for analyzing our selected images are described. Chapter 5 reports the tabulated results of this study followed by the pertaining in-detailed interpretations. Finally, Chapter 6 contains the conclusions, limitations, and some proposed suggestions regarding future work and potential improvements of the applications.

## Chapter 2

### BACKGROUND CONCEPTS AND RELATED WORKS

#### 2.1 Importance of Elastin Lamella in Defining the Micromechanics of Arterial Vessels

The structure of a normal cardiovascular artery consists of three layers: tunica externa, tunica media, and tunica intima. Respectively, each of these layers denotes the outermost, medial, and innermost layer of the artery. Figure 2.1 shows a schematic picture of these three layers in an artery. In the same figure, the axial strip and ring-shaped specimens, which are the two most common shapes of the artery samples, are illustrated. Constructed with concentric elastin lamella, media endows the main mechanical characteristics of the blood vessel [21]. As a result, a closer look at the elastin fibers, elastin layers, and their properties is needed.

Elastin is a single gene-copy protein that accounts for almost half of the dry weight of tissue. Further, this protein is the load-bearing microstructural element of blood vessels. From the structural point of view, the extracellular matrix of the blood vessel tissue predominantly consists of collagen fibrillar, and microfibril elastin. The former serves as the supporting element of tissue, while the latter endows the necessary elastic properties required for efficient stress distribution and dissipation [29].

Based on numerous pathological studies, atherosclerosis and diabetes are two of the main complications highly associated with the impairment of elastin fibers. [23, 26, 15, 7, 30]. Moreover, as a result of the elastin degradation of arteries, arterial disorders can cause serious health issues and cardiovascular diseases. [23]. While the elastin itself is resistant to abnormalities and impairment, degradation and modification of elastin fibers correspond to serious aortic diseases such as aortic dissection, diabetes, and coronary atherosclerosis [6]. Notably, after someone reaches puberty, the rate of synthesis of elastin fibers is almost zero [8]. Therefore, the role of elastin layers in the elastic behavior of arteries with respect to distribution, orientation, and overall morphological properties is of utmost importance for research. Thanks to research efforts, we now know that aging is one of the key factors in the deformation and degradation of these fibers. Based on numerous bio-medical studies, aging is highly correlated with the decrease in the number of elastin lamella and other changes in morphological properties of the elastin layers [25]. The morphological properties of elastin lamella have been investigated exhaustively, but there remains more puzzles to solve regarding the other aspects of elastin layers.

## **2.2 Morphological Properties of Elastin Fibers and Lamella Inside Cardiovascular Blood Vessels**

To study the biomechanical properties of arteries, their mechanical properties should be tested and analyzed. One common approach in determining these mechanical properties is uniaxial tensile testing. As the microstructures of the vascular blood vessels bears tensile stresses, the morphological behaviors of the elastin lamellae during this test can shed light on some underlying causes of

cardiovascular disorders [18].

As previously discussed, a more in-depth analysis of the structure of elastin lamella might provide valuable insights about the resilience of blood vessels and their elastic behaviors. Since unimpaired blood circulation is critical to the performance of arteries, these multicellular organisms should undergo a countless number of dilations and contractions. As defined by Kielty et al., elastic fibers are major insoluble extracellular matrix assemblies, with which suitable resilience and deformability can be achieved [12]. Elastin fibers have a twisted structure with an average thickness of  $0.5\mu m$ . These fibers are more concentrated in the aorta and in the arterial vessels. Therefore, in these dense tissues, the condensed clusters of elastin fibers are more visible in the form of flattened sheets or elastin lamella [29]. As demonstrated by Albert and Spicer et al., elastin fibers consist of microfibrils, which are fiber-like strands that describe the microfibril functionality of elastin fibers [4, 24]. Interestingly, the morphological characteristics of elastin lamellae are highly attributable to the elastic behavior of individual tissues [28]. More specifically, aorta must be resilient to dissipate the blood pressure in a uniform and effective manner. This characteristic is highly associated with the organization of these concentric elastin lamellae.

### **2.3 Automation in Pathology by Using Image Processing Techniques**

In the ongoing study of elastin fibers, practical analysis of histology images, automation and computerization play a key role. In this section, there will be a brief overview of the related work concerning automatized image processing techniques. Not all of these studies are directly related to the image processing

of arterial elastin lamella. However, the proposed methods are in line with the approach of the current research.

One of the image processing techniques for the recognition of elastin fibers and their orientations is the contour detection and ellipse-fitting techniques. Contour detection, also known as edge detection, techniques should be executed once the gray-scale image is filtered for noise by using the Gaussian filtering technique. Tsamis et al. used similar approaches to detect the orientation of elastin fibers in histology images [27]. By focusing on the micro-architecture of the ascending thoracic aortic (ATA) aneurysm media, they hypothesized that the corresponding anomalies in the ATA originate from the morphologic phenotype of the aortic valve. Therefore, they conducted a series of delamination testing to monitor micro-architectural changes in the elastin and collagen fibers. To attempt automated fiber orientation detection, they implemented the Hough transform algorithm in their in-house MATLAB code in order to identify the best-fit line for each fiber. Consequently, they calculated the orientation of the elastin fibers. The result of their study showed that age has a direct effect on the undulated shape of collagen along the longitudinal-radial planes of human ATA tissue. Meanwhile, the elastin orientation becomes more in line with the longitudinal axis. If performed manually, similar to quantifying continuity of elastin lamellae, the results of elastin fiber-orientation detection might not have been as reliable as the ones obtained from the application. The reason lies behind the fact that human estimations of angle and positions of lines are subjected to noticeable error [10]. Additionally, due to personal differences, the consistency of many results that involve geometric judgments would likely be questionable. This line of thought suggests that an accurate, automated approach would serve better as a standard method in fiber position and orientation measurements. Similar to Tsamis et al.s work, Karlon et al.

proposed an algorithm that could reasonably quantify the disorientation level of myofiber. Myofiber, known as a muscle fibril, is the building block of the cellular muscle. The focal myofiber disarray can result in several cardiac complications such as hypertrophic cardiomyopathy. Their study showed that focal myofiber disarray is correlated with certain cardiac diseases [11]. To automatically measure the myofiber disarray, Karlon et al. suggested a multi-step image processing procedure. Their technique consisted of four main steps. First, by implementing the two Gaussian filters, the Difference of Gaussian (DOG) was applied to the picture. This step was imperative for accurately detecting edges of the visible fibers. Second, the 5x5 Sobel filtering function was used to generate four gradient images, and each corresponded to 0, 90, -45, and +45-degree orientation. Third, for each image, they assigned a threshold by which they could convert the image into a binary image. Finally, the orientations of the connected parts were obtained by identifying the connected high-intensity pixels, utilizing the best-fit lines for each contour, and calculating the slope of each line. The results of their algorithm were compared with those calculated manually by using the NIH image software. With roughly 20 percent difference, their automated image processing method indicated a fast, accurate, and reliable alternative to the manual disarray measurements of myofibers.

Given the importance of the extraction and analysis of cells in practical medicine, many researchers invested in the use of image processing techniques to increase automation and accuracy levels of cell analysis. By analyzing the binary image layers, Nedzved et al. strove to find the line of one-pixel thickness to compute the morphological gradient of cell borders [17]. They considered background extraction as one of the essential steps in analyzing medical images. By proposing a new thinning algorithm, they were able to find the ridges of

the cells more accurately than previously suggested thinning algorithms were. The study outcome showed that the proposed segmentation method produced acceptable results in the BIOSCAN system.

Morphological cell detection can be considered useful in grading and treating breast cancers as well. Akin to Nedzved et al.'s study yet enhanced with machine learning techniques (binary tree training), Petushi et al. presented an image processing technique that could automatically classify and grade the histology images of samples susceptible to breast cancer [19]. This approach contained three main steps; namely, gray-scale segmentation, feature extraction, and machine learning model training. By implementing these techniques in their code, the software was able to identify fat cells, stroma, and three cell nuclei types. Three cell nuclei types are crucial for grading cancer. In order to segment the areas of interests, which were mainly cell nuclei, a combination of adaptive thresholding and a series of morphological opening and closing operations were utilized. Petushi et al.'s image processing application was capable of automatically finding the best threshold for segmentation process. Additionally, the smoothing process was performed accurately by filling up the gaps and removing the connected blobs in the image. Considering the reported 90 percent accuracy, their proposed image processing technique reflected a reliable automated approach to classify and grade H& E (Haematoxylin and Eosin) stained slides.

Another interesting topic in edge detection and image segmentation modalities is in the optic neuropathies. Optic neuropathies, such as Glaucoma, negatively affect vision quality and can possibly lead to blindness. To detect the extent to which the optic nerve is damaged, the number of remaining axons must be counted. However, counting the number of axons can be a tedious, prolonged and error-prone task if performed manually. To overcome this time-consuming

process, Reynaud et al. presented a new algorithm in their image processing app with which the counting process could be accomplished swiftly and conveniently [20]. First, all the pixels of the gray-scale images of the optic nerve were classified into myelin (black) or other (white) by utilizing the probabilistic Fuzzy C-mean Classifier. Second, the contours were characterized by fitting ellipses into the black-colored connected parts and later filtered. Finally, the accepted contours were counted as axions, and the resultant value was reported to the user. Compared to the result of the semi-automated image processing performed by an expert operator, their application was able to count axions correctly at a 95% confidence level even with the presence of optic nerve damages.

An additional approach in detecting the edges of the object of interest was presented in Soorya et al.s study on Glaucoma, an ocular disease which may lead to blindness [14]. By employing novel blood-vessel tracking and bend-point detection techniques on fundus images, Soorya et al. submitted a robust automated image processing approach for glaucoma diagnosis that includes a geometrically segmenting algorithm. In their approach, the corners of the blood vessels located inside the disc region were first identified. Second, by connecting the bend points, the contour of the optic cup was obtained. Finally, by measuring the ratio of the vertical cup to the disk, the final decision regarding the susceptibility of the analyzed image to Glaucoma was inferred. The accuracy of such a method in classifying fundus images was 97 percent, a very high degree of accuracy.

In regards to histological image analysis, not only can the enhancement of in-house scripts with the popular image processing algorithms result in accurate and automated image processing applications, but the resultant extracted features can also be used in many classifying algorithms. If implemented wisely, useful algorithms such as thinning, thresholding, Gaussian filtering, Canny edge detection,

and principal-shape fitting can dramatically facilitate and improve the prolonged and time-consuming manual/semi-manual image analysis of histological images.

## Chapter 3

### ALGORITHMS

#### 3.1 Algorithm for Extracting Elastin-Related Features

Every good application is founded upon a good algorithm. Algorithms are the essential parts of any application. In this section, you can find a brief presentation of the main algorithms utilized for extracting and storing intended features of histology images. Later on, we will discuss the whole process in more details.

Pseudocode (applications main algorithm):

```

initialization
// thresholds for black pixel intensity, white pixel intensity,
// number of pixels in a contour and minimum thickness of
// elastin lamellae in micrometer
// Ask the user to input values for these variables
Data: Input blackThre, whiteThre, minThickness, numLineProbe, imageDirectory
1 GET all the names in the imageDirectory
2 PUSHBACK the retrieved names to allNames
3 foreach name in allNames do
4   CLEAR lineProbeArray
5   READ the image with the corresponding name in the directory
6   REMOVE possible gray areas from the surroundings of the image
7   FIT line to the non-white pixels
8   ROTATE the image to become horizontal based on the best-fit line
9   CREATE binary image based on the blackThre and whiteThre
10  RESIZE and STORE the image for later usage
11  BLUR image
    // Gaussian filtering
12  FILTER image
    // find the leftMost and rightMost defining the left and right
    // boundaries of the image
13  FIND leftMost and rightMost
    // find the top and bottom boundary points
14  FINDBOUNDARIES(leftMost,rightMost)
15  CLEAR topBPs and bottomBPs
16  FIT polynomial of degree DEGREE to the topBPs
17  FIT polynomial of degree DEGREE to the bottomBPs
18  STORE the coef. of the polyFit with the least-fitting error
19  while  $i < \text{numLineProbe}$  do
20    SET  $X_i$  to  $(i * (\text{leftMost} - \text{rightMost}) / \text{numLineProbe}) + \text{leftmost}$ 
21    DRAW perpendicular line to the polyFit at  $X_i$ 
22    PUSHBACK COUNT(startPoint,endPoint) into lineProbeArray
23  end
24  FIND the layers' distance distribution
25  FIND the density of black-colored pixels
26  FIND descriptive parameters
27  STORE all the results into a text file
28 end
Algorithm 1: Main algorithm for boundary recognition and elastin-lamellae
counting

```

```

def FINDBOUNDARIES(leftMost, rightMost):
    while i < numLineProbe do
        SET  $X_i$  to  $(i * (leftMost - rightMost) / numLineProbe) + leftmost$ ;
        foreach contour in contours do
            if contour HAS point with x equal to  $X_i$  then
                FIND the top and bottom boundary points;
                PUSHBACK the values into topBPs and bottomBPs;
            end
        end
        INCREMENT i;
    end
    return topBPs, bottomBPs;

```

```

def COUNT(startPoint,endPoint):
    CONSTRUCT line with startPoint and endPoint;
    SET bPixel to false;
    SET layerThick to 0;
    foreach P on the line do
        if bPixel then
            if PValue < blackThre then
                INCREMENT layerThick;
            else
                SET bPixel to false;
                SET layerThick to 0;
                if layerThick > minThickness then
                    PUSHBACK layerThick into tempArray;
                end
            end
        else
            if PValue < blackThre then
                SET PValue to true;
            end
        end
    end
    return tempArray;

```

## 3.2 Development Platform

Histology-Image Analyzer is the name of the proposed application for automatically reading and analyzing the histology images of arteries. The app has been written in C++ and is capable of being executed on any Windows machine device. As for the image processing library, OpenCV [2] library has been implemented in this application. OpenCV is one of the most powerful, versatile, and optimized libraries for analyzing images. While it can be used for Java and Android, the two main supporting languages are Python and C++. As for the IDE, the Microsoft Visual Studio 2015 [3] has been used to develop the C++ codes and integrate the dependent libraries.

## 3.3 Image Processing Techniques

### 3.3.1 Tiff-Extracting Feature

By implementing the LibTIFF [1] library for each selected image, this application is capable of reading all of the images available directories, recognizing the number of channels in the image, extracting pixel values for every available raster, and finally assembling the OpenCV image matrices. Images that cannot be handled by OpenCV matrices will be analyzed differently thanks to the available C++ and OpenCV exceptions. For such cases, the tile-based strategy was used for storing the pixels in memory, manipulating the pixel intensity values, executing image-processing operations, and finally storing the analyzed images. Instead of reading the pixels of a raster all at once, the program will read the pixels in a tile fashion (Usually, besides the raster compression method, images with large file size are compressed in the tile format as well). The application reads the number

of available tiles once, and upon success, will start to read the pixels of each tile. Although this procedure is vital for large image files, the memory limitation of any device and OpenCV make it insufficient for image processing. Therefore, instead of storing the pixels in only one matrix, all the extracted pixels will be stored into two or sometimes four separate matrices. Although the presented technique can increase the image processing complexity, it provides us with the capability of easily handling and analyzing huge histology image files (4 gigabits or more in size).

### **3.3.2 Thinning and Thresholding**

Once the image is converted into its corresponding matrix(CES), then all the image processing techniques can be used. One of the greatest aspects of most histology images is their distinctive (and often white-colored) backgrounds. This feature is essential for many image-processing techniques because the separation of the foreground blood vessel from its uniform background can be performed without too much trouble. Since the backgrounds of histology images in the database were white, the first procedure in background removal was the division of all the pixels into two groups of black and white pixels. To that end, a black and white threshold was used for categorizing pixels. Of note, the color of elastin pixels was black or almost black. For better visibility of elastin fibers, the image-processing filter assigns 255 to the intensity value of the black pixel and 0 to the intensity of the white pixel, swapping the black pixels with white pixels. The result of such thresholding produces an image with all of the non-elastin pixels turned black and unified with the background. You can compare the result of thresholding on a sample histology image of an artery in figure 3.1 and 3.2. While this part was an important step towards fiber recognition, it would be incomplete without

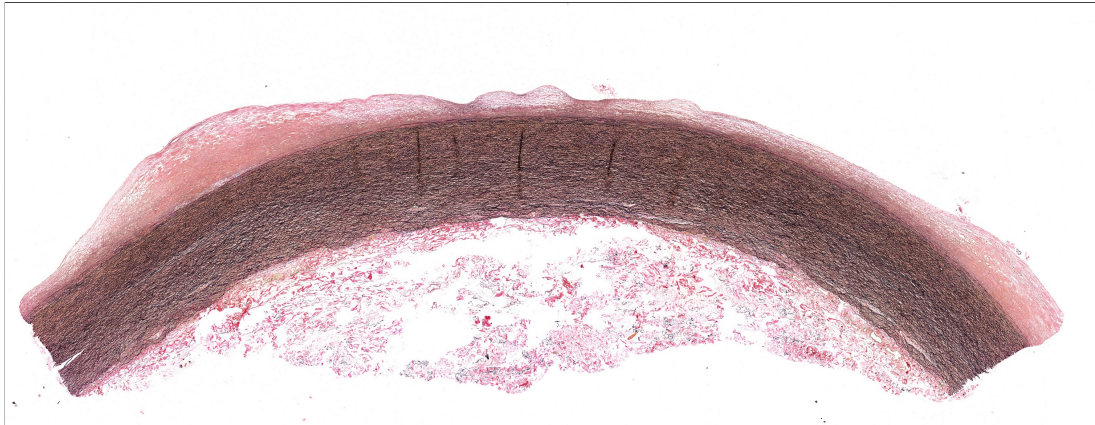


Figure 3.1: sample histology image of an arterial blood vessel

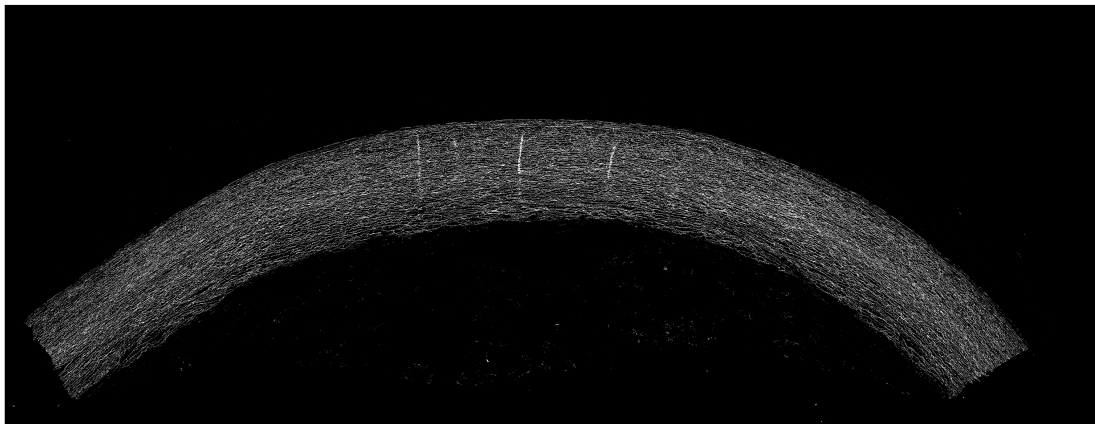


Figure 3.2: the result of black and white thresholding on the blood vessel sample

removing noises from the image. In the next section, we consider and implement the connectivity concept in our image processing technique so that most of the noises would be removed from the histology image.

### 3.3.3 Contour Analysis

In numerous image-processing techniques, using contours is an essential part of the procedure. Contour is a term used for detecting edges [5], or simply, connected pixels. Basically, in a gray-scale image, each contour specifies the set of connected pixels with the same or similar pixel intensities. Therefore, the contour method

will calculate all the boundaries and discretize the image into numerous contours. While the procedure might be time-consuming, the feature can be extremely useful in removing outliers and identifying the object of interest based on the given criteria. Moreover, another advantage of this technique is the accessibility to the pixels grouped by contour vectors.

### 3.3.4 Outlier Removal

The outlier removal can be carried out by using a simple length threshold. In other words, by looping through all the recognized contours, any contour that contains a smaller number of pixels than the assigned threshold will be deleted from the corresponding contour arrays. While this filtering process can be a prolonged task, the final result is promising. If the only goal of contour analysis is outlier removal, then the contours can be searched in the same resized image. In other words, the matrix representative of the original picture will be resized into a new matrix (a new variable), and the contour method will be executed on the resized matrix. This technique is significantly faster than the direct outlier removal with the caveat of transforming or scaling any fitting curve or geometry calculations according to the original image to achieve a correct implementation. As can be seen in Figure 3.3, all the noises presented in the binary image have been removed.

### 3.3.5 Continuity Measurement

As stated in section 1.3, the connectivity feature of elastin lamella is an important elastic characteristic of blood vessels. While contours can effortlessly quantify this parameter, humans would have a hard time performing the same task. This shortcoming in recognition of continuity lies behind the fact that manually detecting boundaries of numerous small elastin fibers is cumbersome or even impossible for

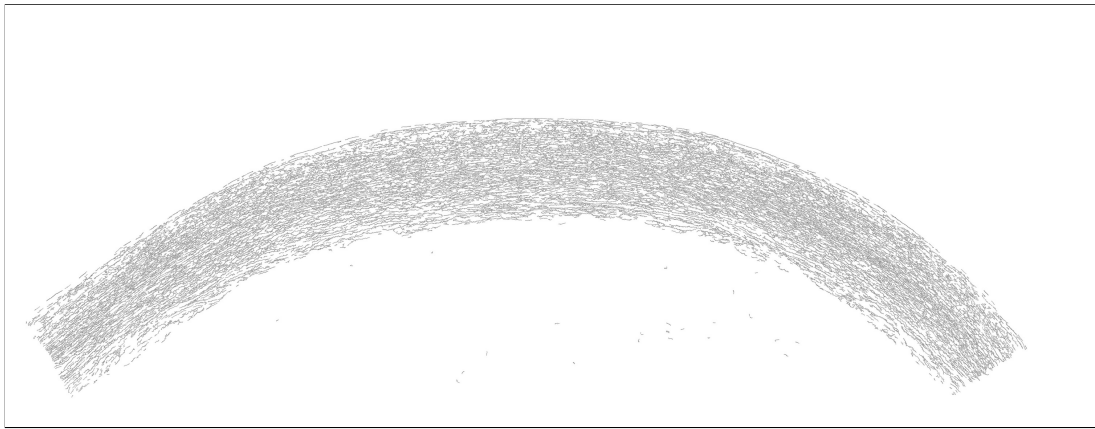


Figure 3.3: the result of black and white thresholding on the blood vessel sample

the human eye. For a specific area in the media layer, there is a strong correlation between the number of black pixels and the connectivity of the elastin lamella. In general, however, a systematic and accurate approach towards connectivity quantification of the elastin lamella would be the normalized number of contours inside the media layer. An additional parameter that can serve as a good indicator of the connectivity of elastin fibers is the average length of the contours for a given area inside the media layer. We must note that although the application currently uses contour detection for outlier removal, connectivity measurement has not been implemented in the application and is planned to be added in the close future.

### 3.3.6 Best-Fit Polynomial

To calculate the number of elastin lamella inside the media layer of arteries, particularly with respect to the distribution of distances between every two lamellae, the orientation of all the image-processing procedures should be directed perpendicular to the blood vessels boundary. To visualize this, we can examine figure 3.4 in which a perpendicular line passes through the media layer and cuts through all of the elastin lamellae. On the other hand, as illustrated in figure

3.5, a non-perpendicular line passes through the blood vessel. As can be seen in this figure, the number of elastin lamellae should not be affected by the angle of the line. However, due to specific shapes of some of the elastin layers, the application overestimated the number of elastin lamella. More importantly, the distance between every two layers has been increased since the distance between the two lines has not been measured perpendicularly.

Now that the importance of perpendicular line probe is emphasized, the focus of the application should be on the techniques that can accurately and consistently probe the elastin lamella with a perpendicular orientation. This orientation should be consistent for all the line probes and throughout the length of the axial or ring-shaped samples. In other words, when drawing many of these line probes (i.e., 200 numbers of line probes), all of them should be equally separated from one another, preferably not intercepting one other, and most importantly, perpendicular to the boundaries of the blood vessel walls. While the boundary points of the vessel can be used to draw perpendicular lines, the lines cannot be consistently drawn right to the boundaries due to stochastic nature of elastin lamella that identifies the boundaries of the vessel, . The problem with this method is shown in figure 3.6.

By utilizing the best-fit curves, the imperfect-boundary-point issue can be resolved straightforwardly. The procedure is as follows: First, by drawing (hypothetically) vertical lines, the boundary points of the horizontalized vessel are identified and stored. Second, by using Vandermonde matrix V, the m-by-(n+1) matrix on the very right side of equation 3.1, the calculation method for the polynomial coefficients can be formulated as follows:

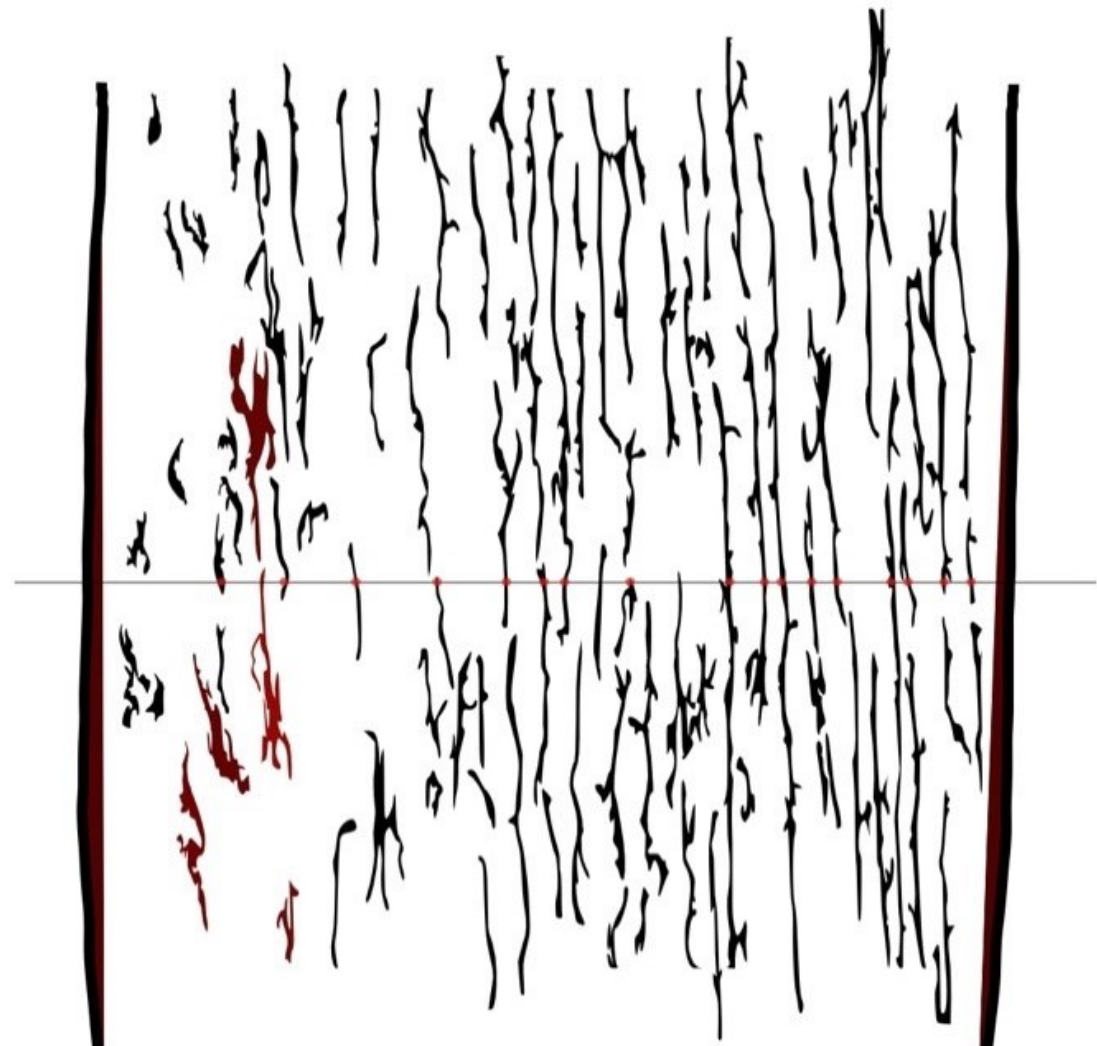


Figure 3.4: A schematic picture of an arteries' walls analyzed with a perpendicular line relative to the blood vessel's direction. Here, the line probe is oriented perpendicular to the boundaries of the vessel. On the other hand, in the left picture, the line probe is not perpendicular to the boundaries, and therefore, not accurately count the number of elastin fibers.

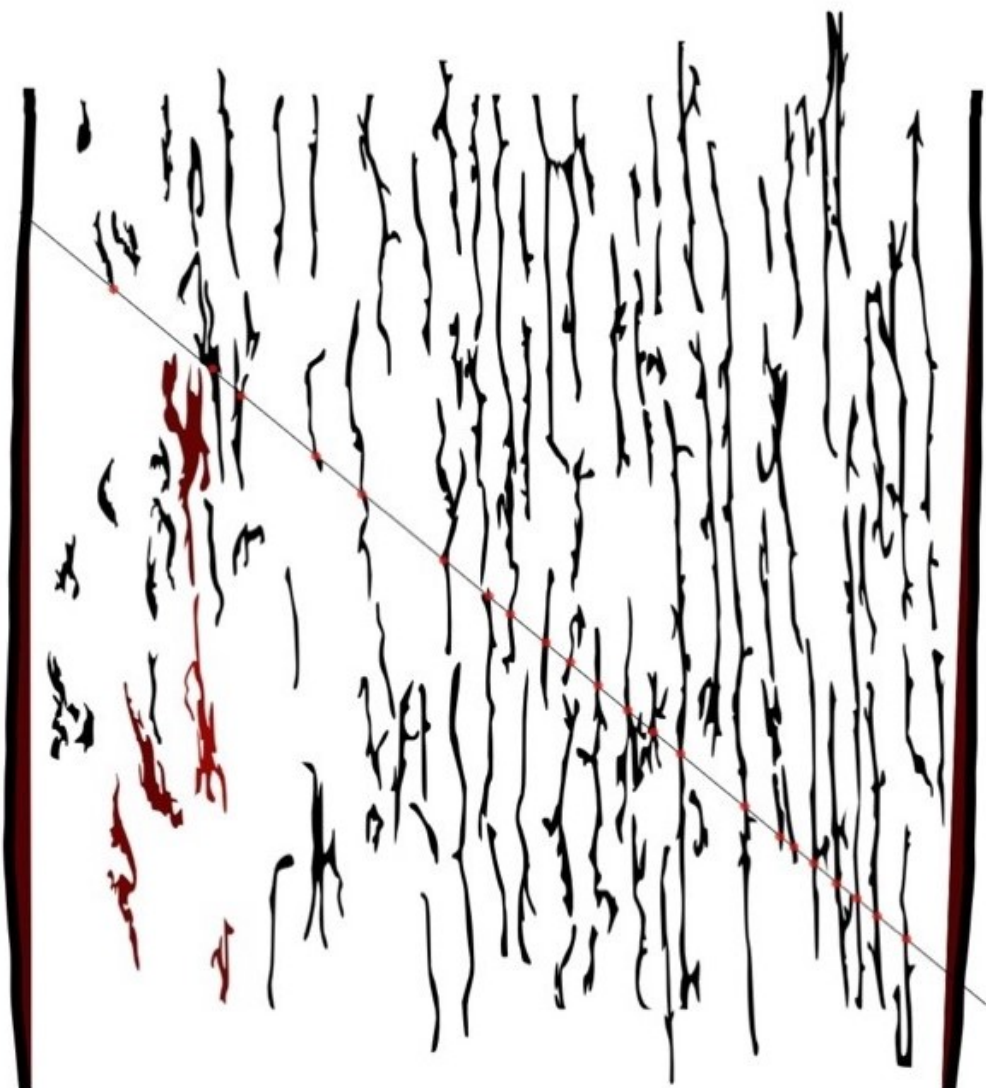


Figure 3.5: A schematic picture of an arteries' walls analyzed with a diagonal line. Here, the line probe is not perpendicular to the boundaries, and therefore, not accurately count the number of elastin fibers.

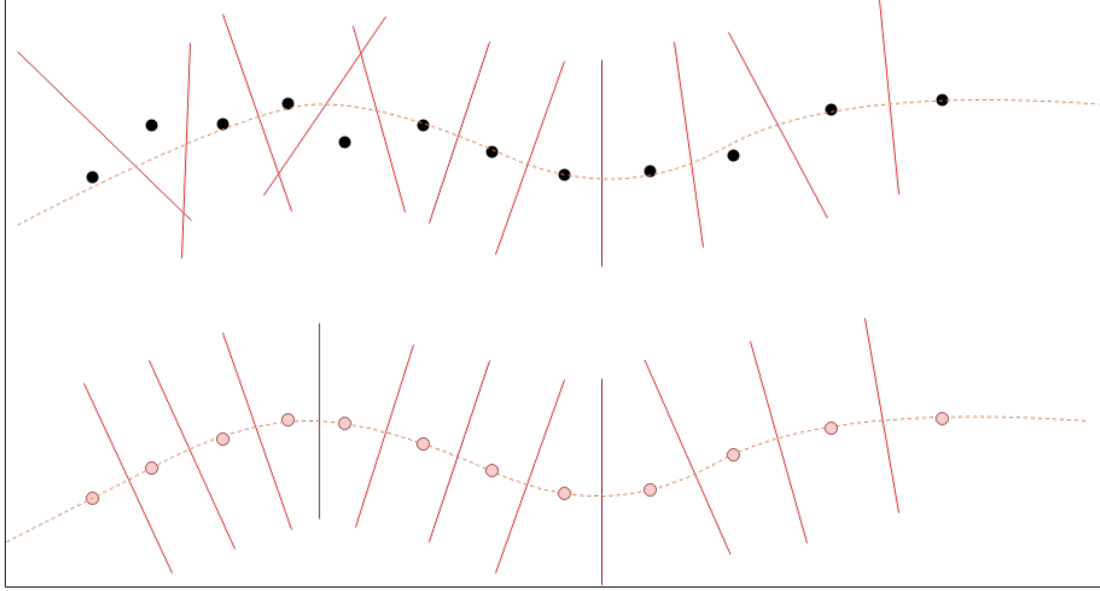


Figure 3.6: Perpendicular line problem due to the inconsistency between the boundary points. At the top, you can see the boundary points used to draw perpendicular lines. At the bottom, the perpendicular lines have been drawn by using a least-square best-fit polynomial of degree 6 that passes through the same boundary points. The red-colored points are the mapped points on the best-fit curve.

$$\begin{pmatrix} x_1^n & x_1^{n-1} & \dots & 1 \\ x_2^n & x_2^{n-1} & \dots & 1 \\ \dots & \dots & \dots & \dots \\ x_m^n & x_m^{n-1} & \dots & 1 \end{pmatrix} * \begin{pmatrix} a_1 \\ a_2 \\ \vdots \\ a_{n+1} \end{pmatrix} = \begin{pmatrix} y_1 \\ y_2 \\ \vdots \\ y_{n+1} \end{pmatrix} \quad (3.1)$$

Although higher degree polynomials might result in a smoother and better fit, one should be very cautious about the susceptibility of such models to extrapolation due to unanticipated turns. Therefore, in the presented application, the polynomial of degree six has been used for blood vessel curve fitting procedures. Once the bounding best-fit polynomials are calculated, the next step would be to draw perpendicular line probes to the boundaries of the vessel. This step can be accomplished easily by considering the array of boundary points on the

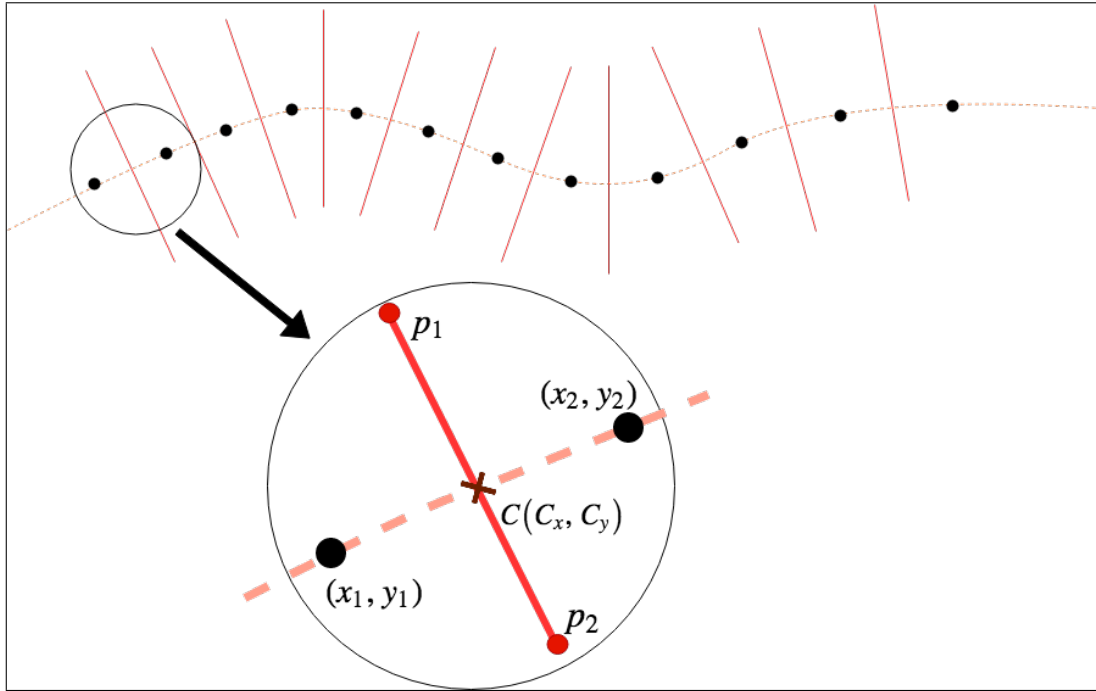


Figure 3.7: The perpendicular lines to the fitted curve along with the points on the curve by which the line probes drew

fitted curve which are equally-separated based on their x coordinates and draw line probes at an angle of 90 degrees to the curve for each pair of adjacent points.

According to equation 3.4, one can programmatically find the center point C for each pair of curve points and draw the perpendicular line to the curve for the value of  $y_1$  and  $y_2$  with a simple sum formula.

$$y_1 = SF * \sum_{j=0}^5 a_j * \left(\frac{x_1}{SF}\right)^{5-j} \quad (3.2)$$

$$y_2 = SF * \sum_{j=0}^5 a_j * \left(\frac{x_2}{SF}\right)^{5-j} \quad (3.3)$$

$$c_x = \frac{x_1 + x_2}{2}, c_y = \frac{y_1 + y_2}{2} \quad (3.4)$$

Here are the formulas for calculating the x and y coordinates of the two points with which the perpendicular line that passes through point c can be constructed:

$$P1_x = c_x + \frac{y_2 - y_1}{\sqrt{(x_2 - x_1)^2 + (y_2 - y_1)^2}} * CONST \quad (3.5)$$

$$P1_y = c_y - \frac{x_2 - x_1}{\sqrt{(x_2 - x_1)^2 + (y_2 - y_1)^2}} * CONST \quad (3.6)$$

$$P2_x = c_x - \frac{y_2 - y_1}{\sqrt{(x_2 - x_1)^2 + (y_2 - y_1)^2}} * CONST \quad (3.7)$$

$$P2_y = c_y + \frac{x_2 - x_1}{\sqrt{(x_2 - x_1)^2 + (y_2 - y_1)^2}} * CONST \quad (3.8)$$

Note that in equations 3.2 and 3.3, SF stands for the scale factor. In curve-fitting methods for large images, this parameter is crucial for scaling down the actual value of the y coordinates. Since the number of pixels in each row of histology images usually exceeds 20,000 pixels, scale factor implementation is a must. Otherwise, higher order terms such as  $a_0(20000)^5$  will result in a noticeable error. One might say that C++ Double variables use 8kb and are adequate for such a task. While the numerical size that can be accommodated in the memory is fairly large for double variables, the number of digits or mantissa is less than 16 digits. This limitation means that, after all the calculations, the final coefficients of the fitting polynomial are not accurate enough. Figure 3.8, 3.9, and 3.10 demonstrate that the precision-problem mentioned above does exist in the curve-fitting procedures for histology images. Therefore, SF implementation is an excellent remedy for the problem of imprecision.

Once the calculation of the y coordinates of the two points is fulfilled, the actual value of the  $y_1$  and  $y_2$  will be retrieved by using the value of SF. Figure 3.11 shows the two best-fitting polynomials that illustrate the boundaries of a blood

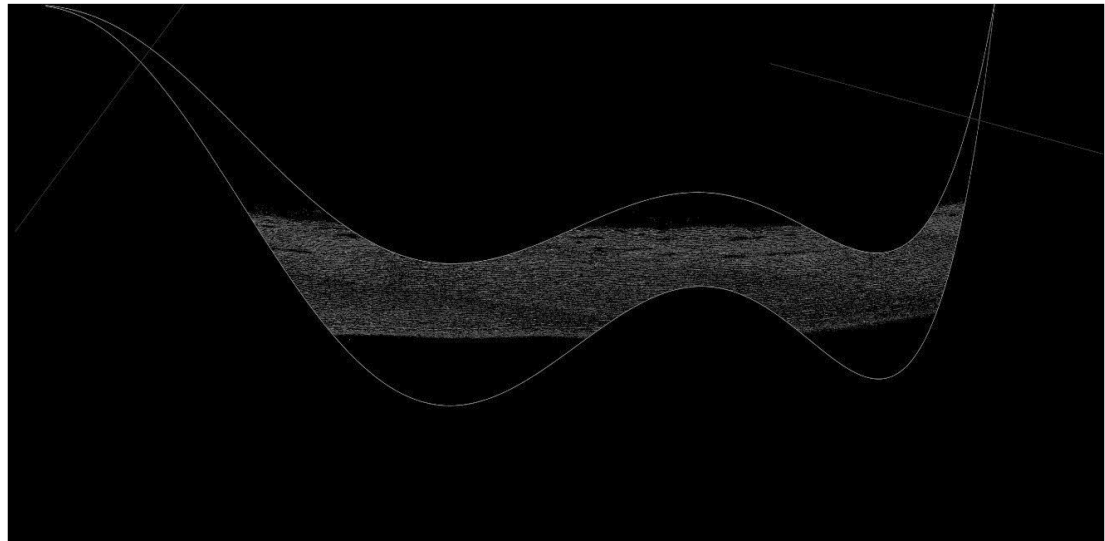


Figure 3.8: The curve-fitting polynomial without any scale factor implementation

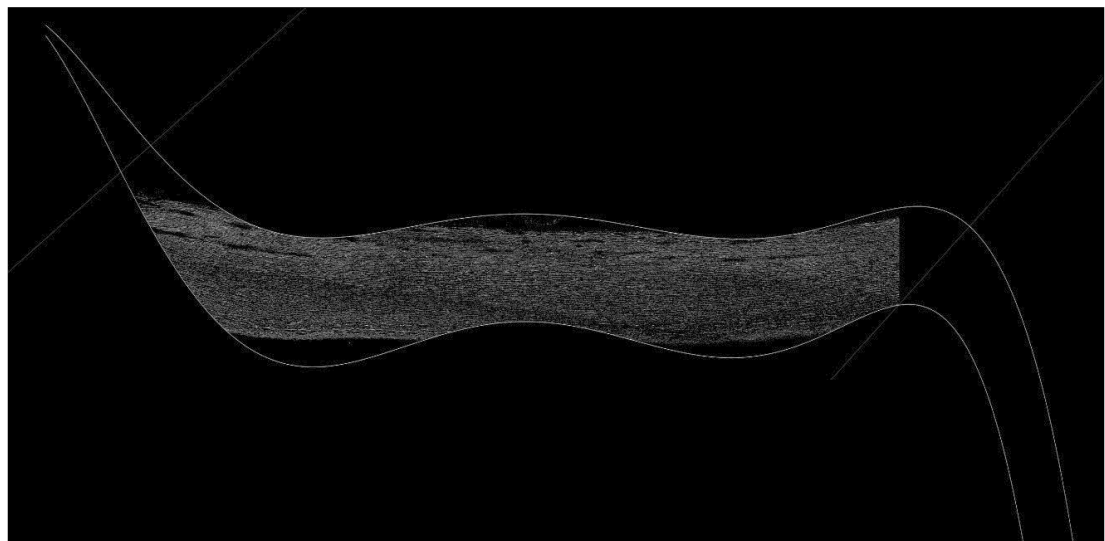


Figure 3.9: The curve-fitting polynomial with the scale factor implementation.  
Here SF is 10.



Figure 3.10: The curve-fitting polynomial with the scale factor implementation.  
Here SF is 100.

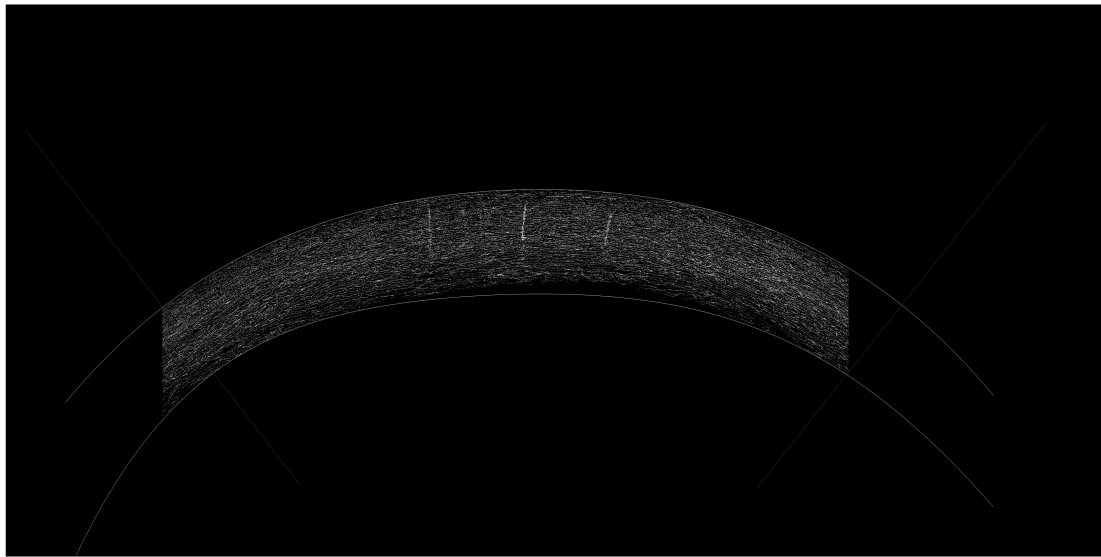


Figure 3.11: The binary image of the artery sample with the two boundary fitting curves

vessel accurately. Similarly, the perpendicular line probes are demonstrated in Figure 3.12.

At this point, our application can successfully remove noises, recognize the boundaries of the vessel, and fit two polynomials of degree five to the top

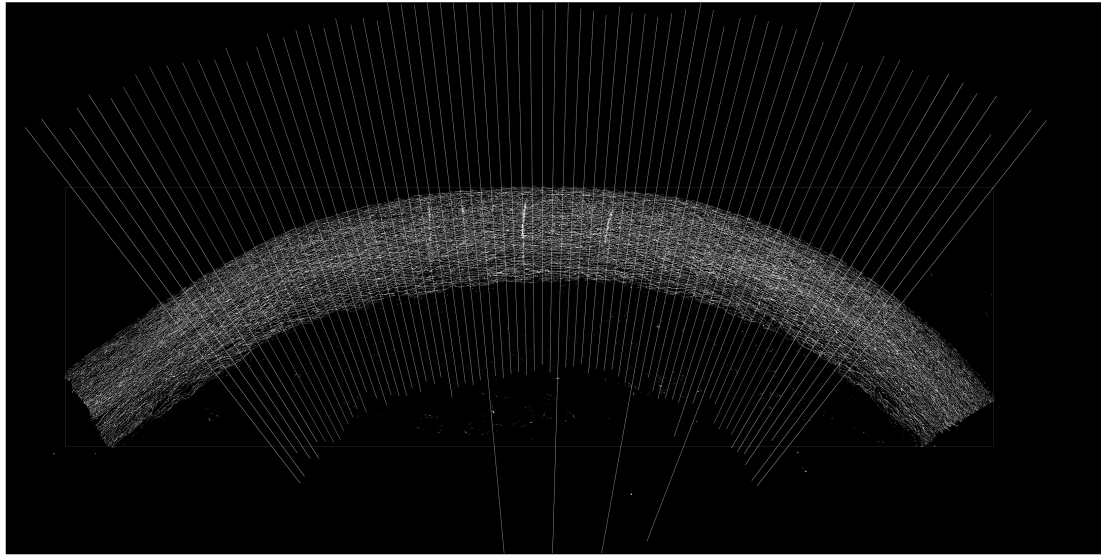


Figure 3.12: The binary image of the artery sample in which the bounding box and the line probe have been illustrated

and bottom of the blood vessel. It is worth noting that the procedures explained above are specifically for axial samples. For the ring-shaped samples, slightly different procedures will be performed. There are one or two minor differences such as using four polynomials of degree five/two for the upper half of the ring, and two for the lower half. Figure 3.13 shows such a case. As can be seen in the picture, the ring-shaped sample cut has been approximated using four fitting polynomials. Due to the extrapolation error and connection inaccuracy of these four polynomials, only the middle part of the ring will be calculated for the black pixel ratio value and filtering purposes.

### 3.3.7 Feature Extraction

Now that the equation of the boundaries of the vessel is calculated, the feature extraction of the media layer becomes possible. By looping through all the pixels of the gray-scale image, those black pixels that have their y coordinates located in-between the corresponding upper and lower points of the best-fit polynomial



Figure 3.13: A ring-shaped cross-section of an artery



Figure 3.14: The image of a ring-shaped sample of an artery bounded with best-fitted curves

will be considered for the computation of the black ratio of media layer (Figure 3.14). Another useful measurement is the average and standard deviation of the thickness of the media layer. These two values are calculated based on the results of the line-probe procedures. Based on the user input for the number of line probes, the application will draw perpendicular lines to the wall of the artery. Then, the first and last acceptable white pixel (elastin) on this line will be stored in the corresponding data structure. A pixel is considered an elastin pixel if the fitting curves bound it. Therefore, for each drawn line, the application goes through all the pixels defining that line. If the first elastin pixels location is in-between the two corresponding fitting polynomials, then the location of the pixel will be saved as the beginning of the media layer.

Similarly, if the last elastin pixels location falls between the bounding polynomials, its location will be stored at the end of the media layer. The pixel scrutiny procedure for finding the boundaries of media layer applies to the fiber counting procedure as well. In other words, for each line probe, media thickness acquisition, fiber counting and space measurement between elastin lamella are calculated in one for loop.

### 3.3.7.1 Layer Counting

Although it might seem straightforward, accurately counting the number of fibers in a histology image can be quiet challenging due to indistinctiveness of elastin layers rooted in the stochastic shape and distribution of elastin lamella (Figure 3.15). Even for specialist operators, this procedure can be difficult to perform. As such, one needs to use some initial assumptions and non-image information to increase the accuracy of fiber detection and counting. The first assumption for detecting an elastin lamellae is the minimum thickness of such a layer. On average,

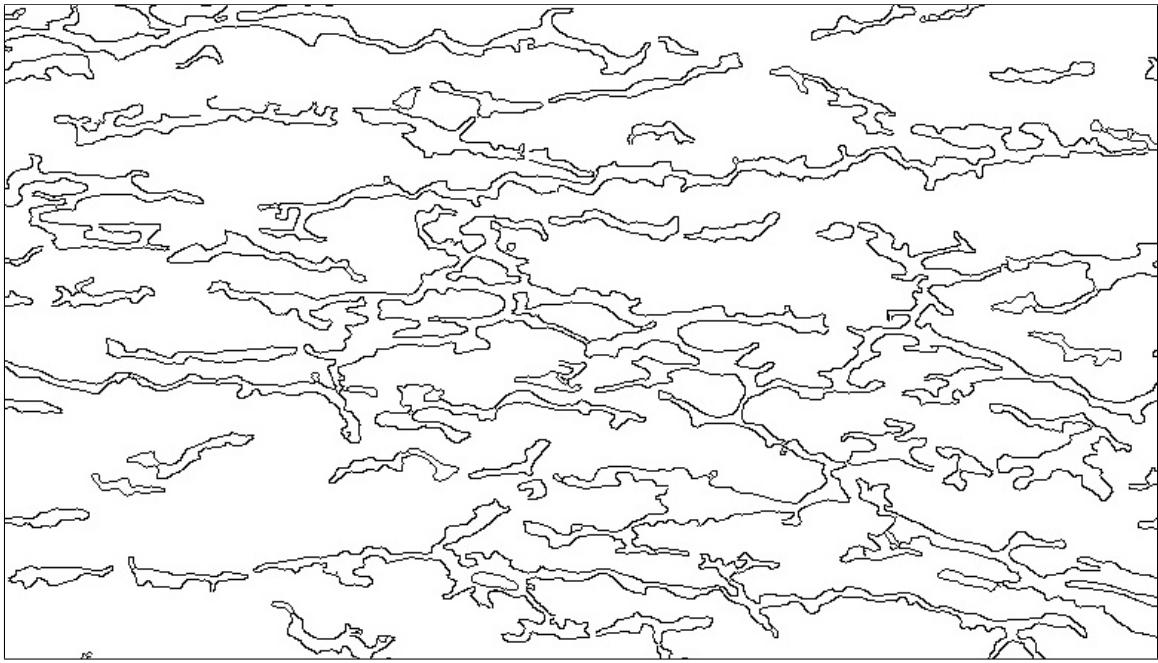


Figure 3.15: A semi-irregular distribution of elastin lamella represented by contours

the thickness of the elastin lamella is close to  $2 \mu m$ . In a  $10x$  histology image, this value corresponds to two pixels. As a result, this could be our threshold for considering a layer as an elastin layer. On the other hand, there is a need for an upper-bound limitation of elastin lamella, so that the two connected lamellae are not accounted for as one elastin layer. One rough estimation of such a value can be the minimum threshold multiplied by two. By applying such a filter to the elastin detection procedure, elastin layers with 5 or more pixels will be split into two minimum thickness layers.

Another approach in elastin lamella counting is the use of contours in detecting layers. Due to the connective nature of contours, two closely connected curves will not be counted as two layers but rather as one layer. On the other hand, finding the start and end pixel points of each layer is challenging and sometimes impossible. Therefore, it seems plausible to move forward with the

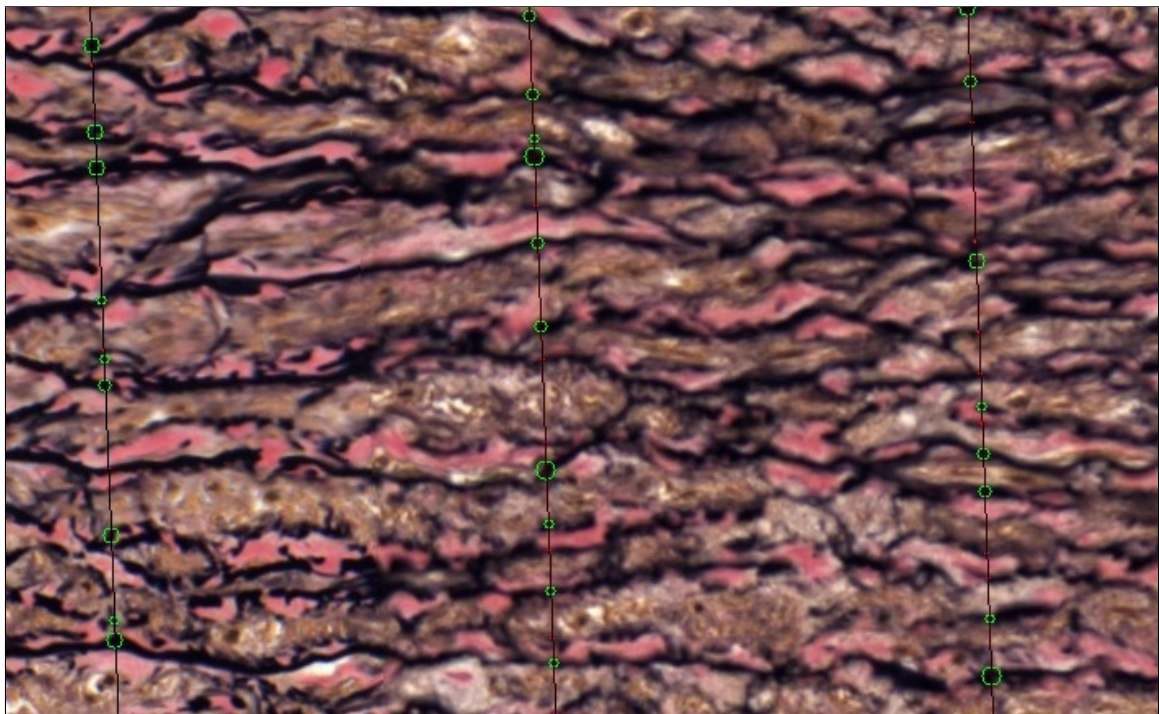


Figure 3.16: The result of elastin lamella detection technique on an artery histology image. In this figure, the tiny red-colored circles (dots) show the non-elastin layers, while the green-colored circles show the elastin lamella.

pixel-probe procedure. By utilizing such a technique, the application was able to detect the elastin lamella acceptably. Figure 3.16 shows the result of such a method in identifying the elastin layers. In this figure, the green circles demonstrate the identified elastin layers, while the small red circles indicate the non-elastin recognized curves.

### 3.3.7.2 Space Measurement between Elastin Lamella

Another important morphological feature of elastin lamella is their distribution along the width of the media layer. Parameters like the average and variability (standard deviation) value of the spaces between two adjacent elastin lamella, along with the average values of the spaces for each quarter of the media layer, can be good indicators of the distribution pattern of these elastin layers. To achieve

these values, the application requires storing the location of the start and end pixel of each recognized elastin layer. This procedure can be executed effortlessly while the application is looking for the elastin lamella. Once all the start and end points of each elastin layer are stored in the pertaining line probe data structure, the space between two consecutive elastin layers can be calculated readily.

## Chapter 4

# METHODOLOGY

### 4.1 Data Source

Histology images were obtained from the Collaboration for Advanced Surgical and Engineering Applications (CASEA) at the University of Nebraska-Medical Center (UNMC). Thirty-one images were randomly selected from a pool of 100 histology images of human aorta axial strips. Each image pertains to a subject. In case of a ruptured blood vessel sample, images of other samples correspond to the same subject were used. All the aorta images were taken by parallel alignment of the samples to the camera lens. In case of slight misalignment, we can use affine invariant image processing technique [9].

#### 4.1.1 Artery Samples

Human aorta blood vessels were obtained from subjects within 24 hours of death. Axial strips of each subject were stained with Verhoeff-Van Gieson (VVG) and scanned at 20x resolution. The VVG stain makes the elastin lamellae visible in the histology images.

Table 4.1: Contingency table for elastin-layer detection

		Gold Standard elastin-layer detection (by operator)	
Algorithm Detection	Detected Non-detected	Detected	Non-detected
		TP FN	FP TN

## 4.2 Histology Image Analyzer Application

Since the Histology Image Analyzer application has been written in C++, the release version of the application is portable and can be run on any Windows machine. Due to the security issue, these high-quality histology images cannot be transported from the database workstation to the computer on which the code was developed. Therefore, the portability of this application is an integral part of the analysis procedures. Once all the image processing analysis has been conducted, the resultant excel files can be copied to an external hard drive for later use. Notably, appropriate exception handlers had been utilized in the application, so that the process of data collection from the batch of the thirty one histology images was performed smoothly and without any crash or stop in the middle of the process.

## 4.3 Gold Standard (GS)

To evaluate the performance of our elastin-layer detection algorithms, the number of elastin lamella computed by the algorithm will be compared with the GS value calculated by clinical experts. The contingency table (Table 1) demonstrates the most frequent evaluating metrics namely Accuracy (Acc), Sensitivity (Se), and Specificity (Sp). Acc, Se, and Sp are respectively the ratio of TP+TN, FN+TP, and TN+FP over the total number of cases (n). The TP, TN, FN, and FP stand for true

positive, true negative, false negative, and false positive, respectively. Although these parameters can be very helpful in explaining the detection capability of image processing algorithms, even the operator might not accurately detect the true elastin layer due to the degradation of elastin layers. Therefore, in this study, the GS is the number of detected elastin layers by the operator that will be compared with the applications result for the number of detected layers. More specifically, the number of elastin layers reported by the operator will be compared with the mode value for the number of detected elastin layers that corresponds to each line probe.

## Chapter 5

### RESULTS AND DISCUSSION

As explained in chapter 4, the number of elastin lamella inside the walls of arteries needs to be compared with the GS investigated by a clinical specialist. Table 5.1 shows the result of the program and the one reported by the operator. Two values need to be considered. First, the mode of the number of elastin lamella for all the line probes in the image; and second, the number of elastin lamella along the imaginary line used by the operator to count the number of layers.

For all the images, the normalized difference between the number of detected elastin layers retrieved once by the program and once by the operator potentially provide a good accuracy index. Another possible accuracy measurement is the average value of all the normalized differences between the calculated and reported numbers for every image.

$$\frac{1}{n} \sum_{i=1}^n \frac{|N_1(i) - N_2(i)|}{N_2(i)} \quad (5.1)$$

$$\frac{|(\sum_{i=1}^n N_1(i)) - (\sum_{i=1}^n N_2(i))|}{\sum_{i=1}^n N_2(i)} \quad (5.2)$$

Formula 5.1 calculates the average normalized differences of the two reported values for each row (i). On the other hand, formula 5.2 computes the normalized

Table 5.1: A part of the programs results for the selected thirty-one histology images corresponding to axial-shape specimens of arteries

row	file name	elastin lamellae			
		by application		manually	
		1	2	3	4
1	Image 1 - TA axial 2ox	79.88	3.45	73	65
2	Image 2 - TA axial 2ox	44.7	4.42	51	53
3	Image 3 - TA axial 2ox	46.8	3.02	41	42
4	Image 4 - TA axial 2ox	133.78	6.25	125	110
5	Image 5 - TA axial 2ox	97.84	4.10	102	105
6	Image 6 - TA axial 2ox	44.88	3.48	47	50
7	Image 7 - TA axial 2ox	66.8	4.11	67	72
8	Image 8 - TA axial 2ox	72.84	3.48	81	79
9	Image 9 - TA axial 2ox	68.76	3.60	68	74
10	Image 10 - TA axial 2ox	30.9	3.73	27	53
11	Image 11 - TA axial 2ox	97.84	4.57	95	91
12	Image 12 - TA axial 2ox	72.8	8.05	71	81
13	Image 13 - TA axial 2ox	58.84	4.68	52	59
14	Image 14 - TA axial 2ox	114.92	5.02	107	106
15	Image 15 - TA axial 2ox	62.92	3.42	61	60
16	Image 16 -TA axial 2ox	78.8	3.99	79	94
17	Image 17 -TA axial 2ox	119.96	4.27	114	102
18	Image 18 -TA axial 2ox	95.5	5.91	97	77
19	Image 19 -TA axial 2ox	70.84	5.21	70	73
20	Image 20 -TA axial 2ox	113.72	4.17	111	88
21	Image 21 -TA axial 2ox	80.8	3.85	83	85
22	Image 22 -TA axial 2ox	74.76	4.26	72	62
23	Image 23 -TA axial 2ox	109.7	4.43	108	92
24	Image 24 -TA axial 2ox	101.4	8.54	95	89
25	Image 25 -TA axial 2ox	128.94	4.86	130	108
26	Image 26 -TA axial 2ox	98.5	7.21	93	91
27	Image 27 -TA axial 2ox	91.8	5.84	91	96
28	Image 28 -TA axial 2ox	84.76	4.67	84	75
29	Image 29 -TA axial 2ox	106.84	4.55	105	97
30	Image 30 -TA axial 2ox	74.96	4.67	68	67
31	Image 31 - TA axial 2ox	105.86	5.67	106	92

Table 5.2: accuracy and consistency test results for the application performance in detecting elastin lamella

Comparison between the GS and program		
	with mode	with the same line probe
Correlation r value	0.91	0.92
Correlation p value	0.00*	0.00*
Normalized differences (%)	2.04	3.72
Avg. norm. differences (%)	13.21	11.54

\* The value is less than 1.7E-10.

differences between the sum of the first and second columns selected for comparison. In these two formulas,  $N_1(i)$  and  $N_2(i)$  represent the values for the row  $i$  of the two compared columns, and  $n$  is the number of images.

In examining Table 5.1, one can ascertain that any high correlation between the values of column 1 and 4 and column 3 and 4 indicate reasonable consistency in elastin counting procedures undertaken by the program. This consistency is essential since many of these image-processing results will be used for statistical comparisons between the subjects. For example, one study might want to investigate the contribution of age to the differences between the subjects density, distribution, and some elastin lamellae. Consistency plays an important role in obtaining reliable results for such a study. Table 5.2 shows the indices mentioned above for measuring the accuracy and the consistency of the algorithms in counting the number of elastin layers.

As can be seen in Table 5.2, the correlation values are close to one for both cases. Statistically supported by significant p-values, these correlation results indicate a strong consistency in the applications approach in counting the number of elastin lamella inside an artery's wall. Furthermore, in counting the number of elastin layers, the accuracy of the algorithms for the average normalized and

total normalized differences are about 90 and 98 percent, respectively. Even though these are favorable results, some elastin layers were not detected by the application, or conversely, some non-elastin black contours (or white depending on the definition) were detected as elastin layers due to the simplicity of the threshold-based algorithms. Figure 5.1, presents an example that demonstrates such scenarios. Due to the thin elastin layers smaller than the threshold, relatively high intensity of the black pixels, and threshold-based algorithm for elastin layer detection, the applications result is accompanied by errors in this image. Although reducing the minimum elastin-layer thickness threshold and increasing the maximum black intensity threshold can mitigate the false skips or false detections of elastin layers, the result of such a change can negatively impact other images with lower black intensity pixels and thicker elastin lamella.

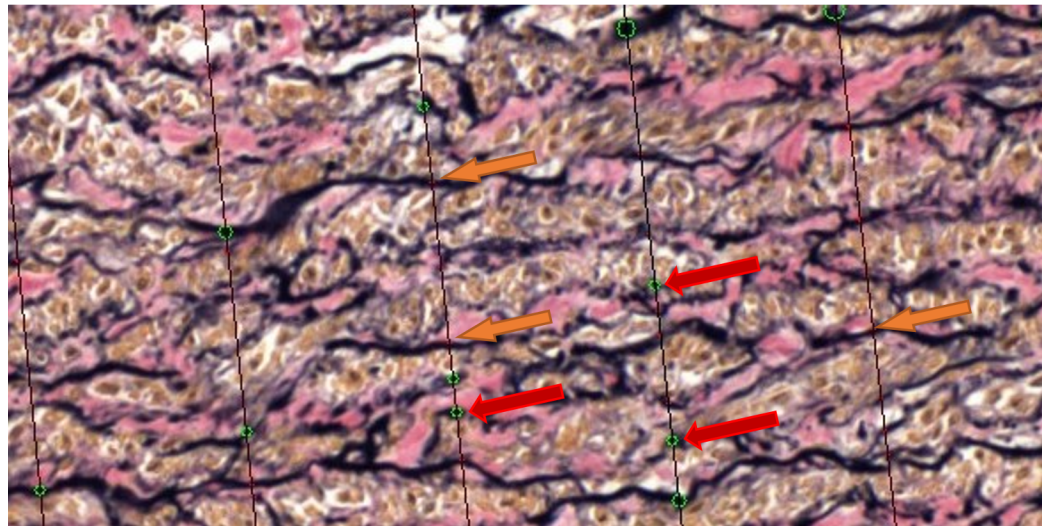


Figure 5.1: This is an example of a bad elastin detection. The red arrows (small head) show false detection, and the orange arrows (big head) show false skips.

One quick fix for this issue might be the use of contour in elastin lamella detection. Since these connected objects can represent elastin layers appropriately, there would be no need for applying the thickness threshold to the counting

algorithms. However, three complications can emerge for such an analysis. 1. Many connected elastin layers will be selected as one connected object so that when the line probe hits the first point of the contour, it will skip over other connected parts of the same contour, which results in a false skip. 2. The contour approach will not work well with low-resolution images. Even the 10x histology images (1 micrometer is 1 pixel) can sometimes cause the contours to connect, which results in elastin false skip and false detection errors. 3. Contour detection is a very time-consuming process. As a result, the duration of analysis can sometimes be magnified by 10. It is important to remember that although the current image processing algorithms use contours for noise detection, the focused image for contour detection is the original image resized with the scale factor of 0.1. Figure 5.2 shows the shape of the contours for the same area illustrated in Figure 5.1.

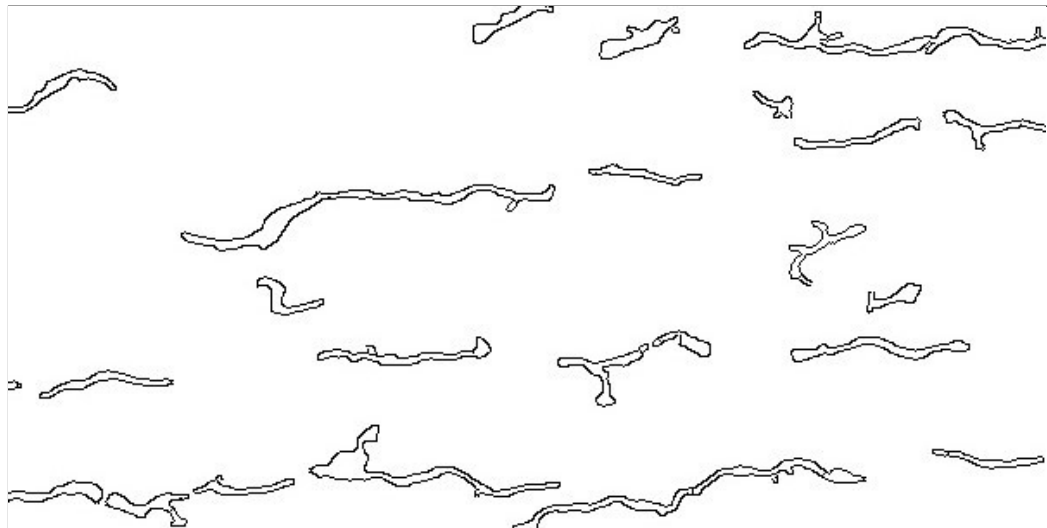


Figure 5.2: Detected contours of black pixels related to a part of a histology image demonstrated earlier on Figure 5.1

Another path in increasing the accuracy of elastin-lamella detection could be to enhance the current approach with the classifying algorithms. Accordingly, the only main difference between our method and the suggested improved method

would be another extra filter for layer detection. Although the process of tracing the continuity of a lamella might be challenging due to the semi-irregular shapes of elastin layers, deep learning methods are believed to be useful in this regard. The popularity of deep learning methods, especially unsupervised or semi-supervised learning methods, is growing fast. The reasons for the rise in popularity lie in the fact that deep learning methods solely extract the suitable features from the image and are not dependent on domain expertise for feature selection unlike their machine learning counterparts. Another reason for the attractiveness of deep learning methods originates from the increasing availability of public datasets containing anatomical images [16].

## Chapter 6

# CONCLUSIONS AND FUTURE WORK

### 6.1 Conclusion

The current study attempted to completely automatize the geometric morphological analysis of elastin lamella inside cardiovascular arteries. Based on the comparison between the result of the application to the Gold Standard (GS), within %10 error, the presented image processing algorithms were able to find the number of elastin lamella in the axial and ring-shaped arteries walls. In addition, the distribution result of the elastin layers was effectively calculated since the start and end points of each layer were obtained during the counting process. Accordingly, the proposed algorithms can be utilized to achieve more complex image processing analyses of arteries along with machine learning and deep learning enhancements.

### 6.2 Limitation and Future work

The first limitation of the study pertains to the usage of the threshold-based algorithm for detecting the elastin layers. Based on the black threshold used for elastin detection, some of the images had fade-out black pixels only recognizable by a higher black limit, i.e., 70. On the other hand, increasing the threshold from

50 to 70 would cause the other images to reveal more pixels that might not exactly correspond to elastin layers. The second limitation of this study was the stochastic nature of the elastin lamella distribution and formation along the width of the blood vessels walls. This probabilistic distribution caused the program to consider a black contour as an elastin layer, which was incorrect. The high number of line probes used to count the elastin lamella might be helpful to mitigate this issue. Finally, the most critical limitation of this study is the threshold-based approach for detecting the elastin layers. As discussed, any connected object with a thickness larger than the elastin layer threshold is considered a separate elastin layer. While the overall accuracy of this assumption is adequate for inferences about some general elastic properties of blood vessels, a more systematic and accurate procedure should be undertaken for the geometry of the continuous part of this candidate contour. In other words, the sole consideration of a portion of a contour might not be as accurate as a more in-depth method of elastin-layer detection that is enhanced by a machine-learning or boundary analysis algorithms. Fortunately, the contour detection along the thickness of the blood vessel is a good start for the implementation of such advanced techniques. Developing and fine-tuning such an enhancement could be an excellent topic for future work. In addition, the contour detection method itself can be improved by using suitable interpolation techniques for digital images [13]. In future work, it may be possible to study the elasticity of blood vessels by using vivo imaging. The continuous monitory of elastins inside arteries requires special computer image processing such as the one currently performed in the contours monitoring of road networks [31].

## Bibliography

- [1] LibTIFF - TIFF Library and Utilities v3.6.1, 2005. [3.3.1](#)
- [2] Opencv Library, 2018. [3.2](#)
- [3] Downloads — IDE, Code, & Team Foundation Server — Visual Studio, 2019. [3.2](#)
- [4] Ernest N. Albert. Developing Elastic Tissue: An Electron Microscopic Study. *The American Journal of Pathology*, 69(1):89, 1972. [2.2](#)
- [5] John Canny and J. A Computational Approach to Edge Detection. *IEEE Transactions on Pattern Analysis and Machine Intelligence*, PAMI-8(6):679–698, nov 1986. [3.3.3](#)
- [6] Huan Chen and Ghassan S. Kassab. Microstructure-based biomechanics of coronary arteries in health and disease. *Journal of Biomechanics*, 49(12):2548–2559, aug 2016. [2.1](#)
- [7] Y. C. Fung and Richard Skalak. *Biomechanics. Mechanical Properties of Living Tissues*, volume 49. 2009. [2.1](#)
- [8] Ellen M. Green, Jessica C. Mansfield, James S. Bell, and C. Peter Winlove. The structure and micromechanics of elastic tissue. *Interface Focus*, 4(2):20130058, apr 2014. [2.1](#)

- [9] Sofie Haesevoets, Bart Kuijpers, and Peter Z. Revesz. Affine-Invariant Triangulation of Spatio-Temporal Data with an Application to Image Retrieval. *ISPRS International Journal of Geo-Information*, 6(4):100, mar 2017. [4.1](#)
- [10] Joseph Jastrow. Studies from the University of Wisconsin: On the Judgment of Angles and Positions of Lines. *The American Journal of Psychology*, 5(2):214, nov 1892. [2.3](#)
- [11] W J Karlon, a D McCulloch, J W Covell, J J Hunter, and J H Omens. Regional dysfunction correlates with myofiber disarray in transgenic mice with ventricular expression of ras. *Am. J. Physiol-Heart C.*, 278(3):H898–906, 1998. [2.3](#)
- [12] CM Kielty, MJ Sherratt, and CA Shuttleworth. Elastic fibres. *Journal of cell science*, 115, 2002. [2.2](#)
- [13] Zhiqiang Li and Peter Z. Revesz. Bilinear and Smooth Hue Transition Interpolation-Based Bayer Filter Designs for Digital Cameras. *International Journal of Circuits, Systems and Signal Processing*, 9, 2015. [6.2](#)
- [14] Soorya M., Ashish Issac, and Malay Kishore Dutta. An automated and robust image processing algorithm for glaucoma diagnosis from fundus images using novel blood vessel tracking and bend point detection. *International Journal of Medical Informatics*, 110:52–70, feb 2018. [2.3](#)
- [15] Thomas O. McDonald, Ross G. Gerrity, Christy Jen, Hao Ji Chen, Kathleen Wark, Thomas N. Wight, Alan Chait, and Kevin D. O'Brien. Diabetes and arterial extracellular matrix changes in a porcine model of atherosclerosis. *Journal of Histochemistry and Cytochemistry*, 55(11):1149–1157, nov 2007. [2.1](#)

- [16] Sara Moccia, Elena De Momi, Sara El Hadji, and Leonardo S. Mattos. Blood vessel segmentation algorithms Review of methods, datasets and evaluation metrics. *Computer Methods and Programs in Biomedicine*, 158:71–91, may 2018. [5](#)
- [17] A. Nedzved, S. Ablameyko, and I. Pitas. Morphological segmentation of histology cell images. *Proceedings 15th International Conference on Pattern Recognition. ICPR-2000*, 1:500–503, 2000. [2.3](#)
- [18] Ruth J Okamoto, Jessica E Wagenseil, William R Delong, Sara J Peterson, Nicholas T Kouchoukos, and Thoralf M Sundt III. Mechanical Properties of Dilated Human Ascending Aorta. *Annals of Biomedical Engineering*, 30:624–635, 2002. [1.1](#), [2.2](#)
- [19] Sokol Petushi, Fernando U Garcia, Marian M Haber, Constantine Katsinis, and Aydin Tozeren. BMC Medical Imaging Large-scale computations on histology images reveal grade-differentiating parameters for breast cancer. 2006. [2.3](#)
- [20] Juan Reynaud, Grant Cull, Lin Wang, Brad Fortune, Stuart Gardiner, Claude F Burgoyne, and George A Cioffi. Automated Quantification of Optic Nerve Axons in Primate Glaucomatous and Normal EyesMethod and Comparison to Semi-Automated Manual Quantification. *Investigative Ophthalmology & Visual Science*, 53(6):2951, may 2012. [2.3](#)
- [21] Johannes A. G. Rhodin. Architecture of the Vessel Wall. In *Comprehensive Physiology*, pages 1–31. John Wiley & Sons, Inc., Hoboken, NJ, USA, dec 1980. [2.1](#)
- [22] Roldano Scognamiglio. Cardiovascular and vascular disease of the aorta. *Clinical Cardiology*, 21(1):69–69, jan 1998. [1.1](#)

- [23] Edward R. Smith, Laurie A. Tomlinson, Martin L. Ford, Lawrence P. McMahon, Chakravarthi Rajkumar, and Stephen G. Holt. Elastin Degradation Is Associated With Progressive Aortic Stiffening and All-Cause Mortality in Predialysis Chronic Kidney Disease. *Hypertension*, 59(5):973–978, may 2012. [2.1](#)
- [24] S S Spicer, R M Brissie, and N T Thompson. Variability of dermal elastin visualized ultrastructurally with iron hematoxylin. *The American journal of pathology*, 79(3):481–98, jun 1975. [2.2](#)
- [25] Hadi Taghizadeh and Mohammad Tafazzoli-Shadpour. Characterization of mechanical properties of lamellar structure of the aortic wall: Effect of aging. *Journal of the Mechanical Behavior of Biomedical Materials*, 65:20–28, jan 2017. [2.1](#)
- [26] Hiroko Tomizawa, Masako Yamazaki, Kiyoshi Kunika, Mitsuo Itakura, and Kamejiro Yamashita. Association of elastin glycation and calcium deposit in diabetic rat aorta. *Diabetes Research and Clinical Practice*, 19(1):1–8, jan 1993. [2.1](#)
- [27] Alkiviadis Tsamis, Juli A. Phillipi, Ryan G. Koch, Salvatore Pasta, Antonio D'Amore, Simon C. Watkins, William R. Wagner, Thomas G. Gleason, and David A. Vorp. Fiber micro-architecture in the longitudinal-radial and circumferential-radial planes of ascending thoracic aortic aneurysm media. *Journal of Biomechanics*, 46, 2013. [2.3](#)
- [28] T Ushiki and M Murakumo. Scanning electron microscopic studies of tissue elastin components exposed by a KOH-collagenase or simple KOH digestion method. *Archives of histology and cytology*, 54(4):427–36, oct 1991. [2.2](#)

- [29] Tatsuo Ushiki. Collagen Fibers, Reticular Fibers and Elastic Fibers. A Comprehensive Understanding from a Morphological Viewpoint. *Archives of histology and cytology*, 65(2):109–126, 2002. [2.1](#), [2.2](#)
- [30] Hannah Weisbecker, Christian Vierlinger, David M. Pierce, and Gerhard A. Holzapfel. The role of elastin and collagen in the softening behavior of the human thoracic aortic media. *Journal of Biomechanics*, 46(11):1859–1865, 2013. [2.1](#)
- [31] Hang Yue, Laurence R. Rilett, and Peter Z. Revesz. Spatio-temporal traffic video data archiving and retrieval system. *GeoInformatica*, 20(1):59–94, jan 2016. [6.2](#)